THE PHOTOGRAMMETRIC RECORD

The Photogrammetric Record 29(146): 241–264 (June 2014)
DOI: 10.1111/phor.12061

DEM QUALITY ASSESSMENT WITH A 3D PRINTED GRAVEL BED APPLIED TO STEREO PHOTOGRAMMETRY

S. Bertin (sber081@aucklanduni.ac.nz)
H. Friedrich (h.friedrich@auckland.ac.nz)
P. Delmas (p.delmas@auckland.ac.nz)
E. Chan (ycha171@aucklanduni.ac.nz)
G. Gimel'farb (g.gimelfarb@auckland.ac.nz)
The University of Auckland, New Zealand

Abstract

Using stereo photogrammetry to obtain digital elevation models (DEMs) for surface topography analysis is becoming popular in hydraulic research, especially for coarse gravel beds. This paper assesses the DEM quality by using a realistic 3D printed gravel-bed model, with known elevations every 0·25 mm, as ground truth. Two Nikon D5100 cameras and non-proprietary photogrammetric software for camera calibration and DEM reconstruction are used for the study. A measured DEM is compared point by point with the ground truth and displays a very high measurement accuracy. The 3D printing of ground truths facilitates fast and versatile evaluation of both the DEM quality and the sensitivity of its errors to changes in surface topography and collection parameters. It has the potential to streamline evaluations of calibration and image quality, as well as error filtering strategies. Ultimately, 3D printed models will help in exploring stereomatching error reductions in occluded regions and defining the most suitable strategy for gravel-bed DEM collection, both in air and through water.

Keywords: 3D printing, close range digital photogrammetry, DEM accuracy, gravel bed, ground truth

Introduction

There is a growing demand for high-resolution topographic data in hydraulic experiments, especially over natural water-worked gravel beds. Fine-scale representations of gravel beds with digital elevation models (DEMs) are becoming more and more important for characterising the range of structures associated with water-worked surfaces (Butler et al., 2001; Qin et al., 2012), and the links between microtopography and interfacial hydraulics (Rice et al., 2014).

Digital stereo photogrammetry is capable of obtaining dense topographic data, in both the laboratory and the field, and over dry and submerged riverbeds (Butler et al., 1998;

2002; Chandler et al., 2001; 2003; Carbonneau et al., 2003; Bertin et al., 2012) with lower cost, greater versatility and higher speed of data acquisition, than alternative surveying techniques. However, as with all these methods, small-magnitude errors are likely to propagate and significantly affect the quality of both the resulting DEM and extracted topographic parameters (Lane et al., 2005), especially with low relief surfaces (Hodge et al., 2009).

To ensure that recorded topographic models suit experimental requirements, it is important to evaluate the overall performance of the recording environment. To do so, the performance of the device and of the chosen methodological approach is represented in terms of DEM quality and can be characterised by a global measure of error (Lane et al., 2005).

Errors should also be investigated at each stage of the recording process, in order to define a means of data collection improvement (Lane et al., 2005; Rieke-Zapp et al., 2009). This is a particular concern for digital stereo-photogrammetric automated DEM generation, as errors can arise from various parts of the process (Lane et al., 2000; Carbonneau et al., 2003; Bertin et al., 2012).

Related Work on the Quality of Topographic Data

The topographic data quality in engineering surveying is described in terms of accuracy, precision and reliability (Cooper and Cross, 1988; Butler et al., 1998; Lane et al., 2000; Carbonneau et al., 2003; Hodge et al., 2009). *Accuracy* is the most commonly employed descriptor (Lane et al., 2005) related to systematic errors in a DEM and generally represented by the mean error (ME) between observed metrics and true values. According to Cooper and Cross (1988), the inaccuracies occur in the measurements due to an incorrect functional model, such as an inadequate lens distortion model in stereo photogrammetry. The measurement *precision* refers to inconsistencies (random errors) between repeated measurements under the same conditions. Such errors cannot be eliminated by refining the functional model or applying corrections (Cooper and Cross, 1988). Most importantly, global precision is traditionally computed using the standard deviation of the errors (SDE). The root mean square error (RMSE) is normally obtained through independent checks on the measured data (Lane et al., 2000; 2003; Butler et al., 2002; Brasington and Smart, 2003; Carbonneau et al., 2003) and will quantify random and systematic errors into a single measure of data quality (Butler et al., 1998; Chandler et al., 2003; Lane et al., 2005). The RMSE is frequently labelled the "accuracy" and assumes that the method of determining the independent checks is superior to the method under consideration (photogrammetry in this instance). Gross errors or blunders, which arise from an incorrect measuring process or malfunctioning equipment, determine the *internal reliability* of the DEM. This descriptor is assessed by comparing semi-independent metrics, such as DEMs obtained using different baselines (Butler et al., 1998), or extracted from different imagery (Brasington and Smart, 2003), or obtained through water and in air (Butler et al., 2002; Smith et al., 2012). The *external reliability* is quantified by comparing a topographic parameter of interest, calculated from the DEM, with a theoretical reference. Such external parameters can be slopes of the measured surface for large-scale DEMs (Lane et al., 2000) or scaling properties of small-scale surfaces (Carbonneau et al., 2003). Whilst tests of the external reliability can be beneficial in investigating effects of changing DEM collection parameters, when accuracy statistics are insensitive, the difficulty resides in defining the reference values for the parameters of interest (Lane et al., 2000).

In practice, the topographic data quality is quantified in both the laboratory and field by comparing metrics contained in a DEM for a small number of check points (generally, less than 1% of all the DEM points), directly over the measured surface. Total stations or alternative measuring devices are usually employed to locate and register the check points within the DEM. Limitations of this approach are positioning errors, low density and arbitrary distributions of the check points. Reliability of the data quality measured with this approach cannot be ascertained, especially over rough surfaces, possibly leading to wrong conclusions about the DEM quality (Butler et al., 1998; 2002; Gooch et al., 1999; Lane, 2000; Lane et al., 2000; Brasington and Smart, 2003; Carbonneau et al., 2003; Chandler et al., 2003; Rieke-Zapp et al., 2009; Smith et al., 2012; Bouratsis et al., 2013).

To improve the check point density, Chandler et al. (2001) measured a rough flume-bed surface with both stereo photogrammetry and laser scanning and compared point by point 5589 homogeneously distributed elevations. However, the laser-scanned and photogrammetric data were obtained using different datums, and whilst data alignment was said to be problematic (Lane, 2000), a detailed procedure was not presented. Additionally, whilst laser scanning over rough surfaces is very accurate in theory, it is not error-free in practice (Hodge et al., 2009). Therefore, each assessment calls for both DEM reconstruction and error editing.

The measurement of objects of known size is another traditional approach to evaluate the quality of topographic surveys (Hodge et al., 2009; Pollyea and Fairley, 2012; Bouratsis et al., 2013). Wang et al. (2009) used a realistic 3D seafloor model of known elevations to evaluate laser-scanning and photogrammetric capabilities in measuring seabed roughness. The seafloor model was built with a computer-assisted milling machine achieved a 1 mm sampling distance between the check points and 0·1 mm vertical accuracy. However, whilst the model mimicked the seafloor topography, its all-white surface had an unnatural appearance and lacked texture, resulting in adverse photogrammetric measuring conditions. Additionally, Wang et al. (2009) had to align check points with the observations, which hindered point-by-point comparisons and computation of accuracy. Instead, external reliability measures were evaluated, with the advantage that a reference value for an external parameter (roughness spectrum) could be calculated from the known elevations of the seafloor model.

Whilst the above studies made significant progress on the DEM quality evaluation, additional work is still needed to ensure that derived data-quality measures are sufficient to evaluate a DEM collection strategy and allow for optimising the recording process. At present, DEM evaluation strategy recommendations are twofold: confidence in check points, their density and uniform distribution over the surface; and correct alignment of measured and true values. The evaluation also needs to be improved for use in different environments.

Paper Overview

In this work a novel methodology for assessing DEM quality was developed and applied to laboratory gravel-bed DEMs collected with digital stereo photogrammetry. Initially, a 3D printed model of known dimensions was produced, based on the experimental stereo-photogrammetric pre-measuring of spatial topography and the visual appearance of a water-worked gravel bed. The dense and uniformly distributed grid of check points from the 3D printed gravel-bed model acted as ground truth for assessing the subsequent stereo-photogrammetric measurements. Adaptive surface de-trending and search means were implemented to align the measured and ground-truth data, thus enabling reliable point-by-point comparisons. The 3D printed model was then assessed as to its ability to

reveal variations in DEM collection parameters, based on the parametric "DEM sampling distance", and how representative the derived accuracy statistics were.

METHODOLOGY

Measurement Environment and General DEM Collection Process

The DEM acquisition environment and the photogrammetric workflow (Table I) are identical to the earlier work by Bertin and Friedrich (2014) on monitoring gravel beds at the grain scale. A purpose-built hydraulic flume (19 m long, 0·5 m wide and 0·5 m deep, with a slope set to 0·5%) has been used for the measurements. A 1 m long, full-width sediment recess 14 m downstream from the inlet was used to prepare the water-worked gravel bed. The evolving gravel-bed topography was recorded through air after the flume was drained.

A gantry-mounting system, sliding on a rail, allows the cameras to be rigidly attached horizontally above the test section. The stereo-photogrammetric set-up comprises two Nikon D5100 cameras with 16·2 Mpixel complementary metal oxide semiconductor (CMOS) sensors (4928 × 3264 pixels) and Nikkor 20 mm fixed-focus lenses. The baseline between the two cameras, and the set-up "flying" height, are adjustable within the ranges 200 to 400 mm and 400 to 1000 mm, respectively. To minimise the effects of gravel protruding and shadowing the surroundings, the two cameras are mounted in a canonical vertical photogrammetric configuration, assuming parallel optical axes directed vertically toward the centreline of the flume.

The lighting consists of two pairs of 1 m long neon lights (58 W with carbon dioxide), placed horizontally on each side of the flume, one light above the other. White Plexiglas sheets at the transparent flume sidewalls diffuse the lighting, creating a more homogenous illumination. The gravel-bed test section is thus illuminated by a "cool daylight" colour. Two additional neon lights, which hang above the flume, are used during the acquisition of

TABLE I. The workflow used for collecting, processing and assessing photogrammetric data. RSEV is the repeat stereomatching error value.

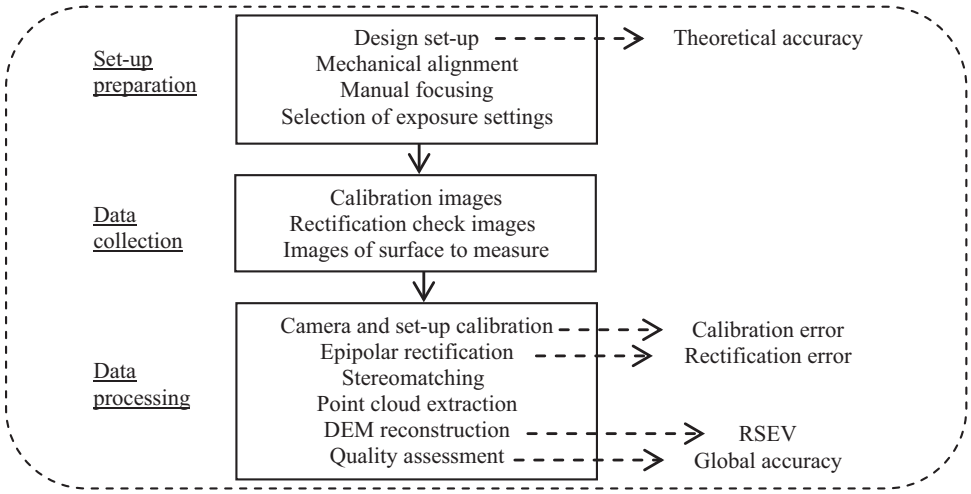

the calibration images. In order not to cast shadows on the surface, these latter lights are turned off for image acquisition of the gravel bed.

The general DEM collection process is presented in Table I and explained in detail below.

(1) The design of the stereo set-up is the first step in a photogrammetric project. It constrains the theoretical accuracy achievable by the set-up, and is thus critical to the success of the measurements (Lane, 2000; Lane et al., 2001). A MATLAB® routine, where the standard central perspective projection equations (pinhole camera model) are implemented, forms a systematic approach to determine the optimum camera-to-object distance (the distance resulting in the best measurement resolution), which complies with the experimental requirements of the measurement window size. Since DEM errors increase near the edges (Butler et al., 2002), a margin around the desired measurement window is commonly accounted for in the design and removed from the DEM during analysis.

(2) During image acquisition, each camera is connected to a computer, allowing remote control and live view with Nikon Control Pro 2® software. This helps to manually focus on the object to be measured and to mechanically align the cameras. After these steps, it is necessary to ensure no modification is made to the physical set-up for the duration of the experiment. Adequate selection of the camera settings is important, as the crucial element to a successful close range photogrammetric process is attaining "good photographs" (Matthews, 2008), where the term "good" refers to pictures that have uniform exposure with high-contrast sharp images. Since the lighting environment will constrain the potential camera settings, it is important that both the lighting environment and the exposure settings are optimised in common as an interdependent pair. To obtain the best quality photographs, the cameras are operated in manual mode. With the Nikkor 20 mm lenses, a combination of an aperture of f/8 (sometimes increased to f/10 or f/11) with a generic sensitivity value such as ISO 200, ensures a good depth of field, a reduced chance of vignetting and sharpness across the image. Once the aperture and ISO are set, these settings must remain constant throughout the acquisition of all images. The shutter speed can be changed to adapt to different lighting conditions.

(3) The camera and set-up calibration is performed using the camera calibration toolbox for MATLAB®, developed by Bouguet (2010). This technique relies on the calibration method of Zhang (1999), whereby calibration parameters (both intrinsic and extrinsic) are computed from a series of photographs of a planar chequerboard in different orientations. Radial distortion (up to the fourth order) and tangential distortion are also modelled during the calibration. Using the calibration results, all stereopairs obtained with the set-up in the calibrated configuration can be rectified to epipolar geometry, where corresponding pixels are on the same scan-line. Image rectification (Fusiello et al., 2000) is included in the calibration toolbox. It should be noted that the toolbox transforms images to greyscale equivalents during rectification, but the code can easily be modified to obtain rectified images in red/green/blue (RGB) format.

(4) Stereomatching is performed on the rectified RGB images using the symmetric dynamic programming stereo (SDPS) algorithm (Gimel'farb, 2002), providing both the grey-coded depth maps and ortho-images for a reconstructed DEM. The SDPS matches corresponding points by minimising pixel mismatches along each scan-

line in the stereopairs. Compared with previous photogrammetric applications in hydraulic experiments (Butler et al., 1998; 2001; 2002; Gooch et al., 1999; Lane, 2000; Lane et al., 2000; 2003; 2005; Chandler et al., 2001; 2003; Brasington and Smart, 2003; Carbonneau et al., 2003; Bouratsis et al., 2013), the SDPS matching is not "area-based". Hence, the DEM smoothing will be less, and the sampling distance can be chosen, if necessary, as small as the pixel size at the object's distance. The SDPS search for the corresponding pixels is bounded by a disparity search range, calculated during the design by predetermining the surface elevation ranges. Post-processing by median filtering, a common practice in photogrammetric surveys (Carbonneau et al., 2003), is applied to eliminate blunders in the depth maps. Using the default filter width of 3 pixels and height of 11 pixels, each given pixel elevation is replaced by the median value over a 3×11 neighbourhood around the corresponding pixel position in the input image. In terms of the matching precision, the SDPS is able to distinguish disparity layers up to 1 pixel, which will give the theoretical depth resolution achievable by the set-up after the pixel size is determined in the object space (see Table III).

(5) From the depth maps and the calibration results, point cloud text files, containing the 3D object coordinates of each pixel in the depth maps, are extracted. The points in these clouds are not regularly spaced, because they pertain to different disparity levels. Using the function "gridfit" in MATLAB®, the point clouds are interpolated (using the default triangle interpolation) into regular grids, with adjustable spacing, and represented as 2·5D DEMs with normalised elevations.

Preparation of a Realistic 3D Printed Gravel-Bed Model

Grain sizes are frequently quoted as D_i, which is the grain size at which the specified percentage i of the grains are finer (so D_{50} = 10 mm means 50% of the grains are smaller than 10 mm). To ensure that the 3D printed model mimics the topography of gravel beds simulated in hydraulic laboratory experiments, a standard sediment mixture, with a median size of the intermediate axis D_{50} = 7·3 mm, a minimum size of 0·7 mm, a maximum size of 65 mm and a geometric standard deviation of the grain size distribution, calculated as $\sqrt{D_{84}/D_{16}}$= 2·98, was used to create a screeded gravel bed in the hydraulic flume. The sediment was water-worked with a flow rate of 60 l/s and a constant water depth of 200 mm, until no sediment movement was observed. The water-worked surface presented evidence of armouring, with a general coarsening of the sediment. The grain size distribution was re-estimated using an orthophotograph of the surface and the image-based method developed by Detert and Weitbrecht (2012), called BASEGRAIN®. It was found to have a D_{50} of 13 mm and $\sqrt{D_{84}/D_{16}}$= 3·25.

Digital stereo photogrammetry was chosen for data collection, as it was the available technique to allow the best compromise between measurement resolution and theoretical

TABLE II. Characteristics of the realistic 3D gravel-bed model (ground truth).

Size (mm)	296 × 184
Sampling distance (mm)	0·25
Number of points with known elevation	873 345
Standard deviation of surface elevation (mm)	5·5
Surface elevation span (mm)	32·6

TABLE III. Summary of the photogrammetric set-up designed for the test. All values were theoretically determined using the design equations and the rounded camera-to-object distance. Actual values may deviate because of the difficulty, in practice, to accurately set the cameras' "flying" height and baseline.

Rounded camera-to-object distance (mm)	636
Common field of view (mm)	500 × 498
Baseline (mm)	250
Range of disparity for 50 mm elevation span (pixels)	1580 to 1710
Overlap (%)	67
Sampling distance (mm)/resolution (pixel/mm^2)	0·15/43
Theoretical vertical accuracy or minimum measurable depth (mm)	0·39
Number of pixels in the 450 mm × 400 mm measurement window	≃7 800 000

depth accuracy (Bertin and Friedrich, 2014). For obtaining the ground truth, two Nikon D90 cameras with Nikkor 18–105 mm lenses were experimentally set up with a baseline of 300 mm and a camera "flying" height of 575 mm. The resulting pixel size on the gravel-bed surface was 0·18 mm, the overlap was 60% and the theoretical depth resolution was 0·35 mm.

Limitations due to the 3D printer restrained the size of the ground truth to 296 mm and 184 mm along the flow and transverse directions, respectively. However, surfaces of this size and smaller have been shown to be suitable for characterising grain-scale surface properties of laboratory gravel beds (Marion et al., 2003; Ockelford and Haynes, 2013). Photogrammetric data were interpolated on a regular grid with a 0·25 mm sampling distance, generating 873 345 points of known elevations (Table II). To facilitate the assessment of future data using the 3D printed model, 5 mm squares at the four corners were made flat, and elevations were normalised to have a mean value of zero and stored in the *ground-truth elevation matrix* (of data size 1185 × 737). Additionally, before sending it to the 3D printer, the DEM was rendered as a hollow object by replicating the surface 5 mm below the original and connecting the two with prolonged edges. The 3D DEM (Fig. 1) was finally transformed in a stereo lithography (.stl) file and sent to the 3D printer.

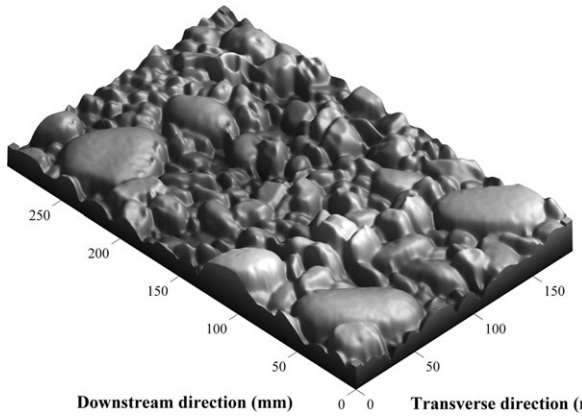

FIG. 1. DEM of a representative patch of gravel bed, of size 296 mm × 184 mm, and 0·25 mm sampling distance, selected for 3D printing.

A ProJet® 3500 HDPlus from 3DSYSTEMS, available at The University of Auckland, was employed for the manufacturing. 3D printing is an additive process, where successive layers of material, VisiJet® Crystal (described as a transparent plastic), are laid down in different shapes. The gravel-bed model was built in approximately 15 h, with a manufacturer's specified accuracy range of 0·033 to 0·066 mm. After manufacturing, the model was left to dry. During the drying process, the edges of the model experienced a minimal upwards curvature due to thermal contraction of the material. The model was therefore mounted onto a flat Perspex plate, ensuring a planar 3D datum.

Preliminary tests showed that stereomatching of images of the 3D printed model does not perform well because of the transparency of the material and weak texture, in other words the lack of contrast and patterns on the surface (Fig. 2(a)). The surface was subsequently finished (Fig. 2(b)), maximising the chance of correctly matched pixels. This was an important step to allow the investigation of the joint effect of topography and DEM collection strategy on the DEM quality, with minimal influence from surface-dependent stereo correspondence problems. Similarly, images of natural gravel beds contain fine texture for successful stereomatching (Butler et al., 1998; Bertin et al., 2012).

Surface finishing was achieved by painting the model in matte black to make the object opaque. Very fine sand ($D_{50} < 0{\cdot}2$ mm) was spread on the freshly painted surface so that, due to the contact with the paint, a single layer of sand attached to the surface. Theoretically, the addition of this real texture altered the initial topography contained in the ground-truth elevation matrix. However, the impact on the assessment of measured data was neglected as: (a) the addition of sand can be approximated by a uniform shift in bed elevation, which is suppressed when the measured DEM is vertically aligned with the ground-truth DEM; and (b) the sand layer thickness is smaller than the minimum depth measurable by the photogrammetric set-up developed for the laboratory experiments (Table III).

EXPERIMENTS

Implementation of the Measurement Technique

This section reports on the particular photogrammetric set-up that was evaluated with the 3D printed gravel bed. The set-up was designed to comply with a desired measurement window of size 450 mm in the flow direction and 400 mm transversely. The baseline between the cameras was set experimentally as close as possible to 250 mm. This was

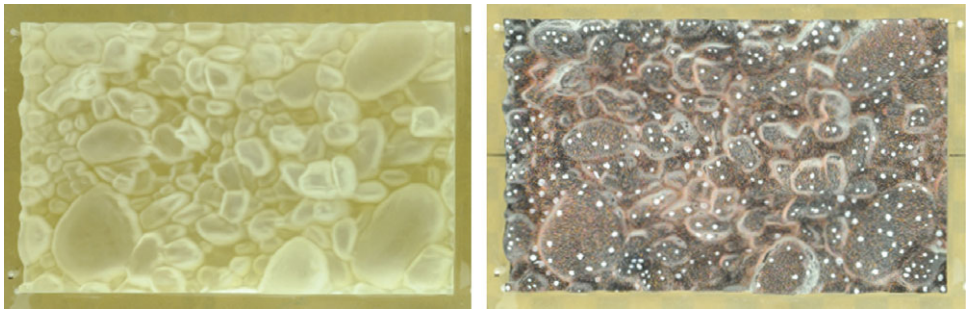

(a) (b)

FIG. 2. Photographs of the 3D printed gravel bed: (a) the raw model; (b) the rendered model.

confirmed after stereo calibration by a numerically estimated 3D distance between the two cameras of 250·3 mm. A 50 mm margin around the measurement window was accounted for and cropped before analysis. Table III summarises the resulting measurement specifications. JPEG (1:4) fine format was selected for the image recording. An aperture of f/10 and sensitivity of ISO 200, combined with a 1/15 s exposure time, allowed good contrast and dynamic range, while manual focusing ensured sharp images.

Data acquisition consisted in obtaining:

(1) 30 stereopairs of a calibration chequerboard covering the whole cameras' common field of view (CFoV) and at distances close to the camera-to-object distance;
(2) 10 additional calibration stereopairs to evaluate the rectification error after calibration;
(3) five stereopairs of a gravel bed; and
(4) five stereopairs of the 3D printed model.

The number of images used for each case is independent of that employed in the other cases. For the camera and set-up calibration, it has been shown that it is essential to have numerous control points (Carbonneau et al., 2003). Further tests, specific to the calibration method employed, revealed that the calibration error reaches a minimum with 20 or more calibration images. The rectification error was spatially determined over the whole CFoV by using 10 additional calibration images. Finally, five stereopair images of the measured surfaces (3D printed model and gravel bed) allowed an investigation into the effect of different imagery on stereomatching results (see the section "Assessment of Stereomatching Reliability" for information on the images). In addition, restricting the number of images to five allowed for a time-efficient process to collapse the individually extracted DEMs into one, with the aim of reducing stereo correspondence gross errors.

Variation of DEM Sampling Distance

The visual aspect and quality of a DEM is strongly impacted by the sampling distance with which the DEM is represented (Lane et al., 2000). Too coarse a point spacing results in a loss of topographic information. At the same time, grid size directly influences the size of the numerical dataset that needs to be handled. A point spacing which is too fine will slow down the calculations. Although, the stereo-photogrammetric system allowed sampling distances as small as 0·15 mm (Table III), the default value for grid spacing was set to 0·25 mm, which is the same sampling distance used for the 3D printed model. The sensitivity of the DEM quality to changes in the collection parameters was evaluated by re-collecting the DEMs using different values for the parameter (sampling distance of 0·5, 0·75, 1, 1·5 and 3 mm).

Quantitative Assessment of DEM Quality Using the 3D Printed Gravel Bed

For assessing the measurement quality, the measured DEM of the 3D printed gravel bed needed to be aligned with the ground-truth DEM. Data alignment had to be performed separately to the DEM reconstruction process, since no means was used to register measured DEMs within a common coordinate system with the ground truth. The data was aligned as follows:

(1) the 3D printed model was placed horizontally in the hydraulic flume at the location where the gravel bed is normally recorded, with its long axis parallel to the cameras' baseline;

(2) horizontal alignment is performed with a search algorithm to find the region where the 3D printed model is represented in the measured DEM; and
(3) vertical alignment makes use of surface de-trending algorithms to remove any tilt between the measured and ground-truth DEMs.

In cases where the sampling distance of the measured DEM is not 0·25 mm, elevations are interpolated onto a 0·25 mm grid to allow comparison with all check points contained in the 3D printed model. Finally, measured DEMs of the 3D printed model are quantitatively assessed after point-by-point elevation comparison with the ground-truth DEM, providing measures of DEM quality.

Any vertical misalignment of the cameras, with the baseline not set parallel to the mean surface of the 3D printed model and/or when the cameras' optical axes are not perpendicular to it, results in systematic comparison errors. This translates to a DEM of difference (DoD) between the measured and ground-truth elevation maps that exhibits a linear trend when the cameras are tilting along one (nominally) horizontal axis and a bilinear trend when they are tilting along both axes (Fig. 3(a)). The trend corresponding to the deviation from the correct position is estimated by fitting a bilinear surface to the DoD in a least squares method (Fig. 3(b)). This surface is then removed from the measured DEM to perform the vertical alignment. The scale in Fig. 3(b) indicates that the vertical misalignment is responsible for systematic elevation discrepancies of up to several millimetres. It is thus fundamental to remove the misalignment before a realistic assessment of the measured DEM can be undertaken.

The reliability of the vertical alignment process was assessed by comparing the trends extracted from DEMs collected using a 0·25 mm (Fig. 3) with another employing a 3 mm sampling distance. The latter is the coarsest grid used in this study and thus it was expected that differences between the two trends would be maximised for this case. The vertical alignment was reliable, as even for the coarsest grid the mean unsigned (absolute) difference between the two estimated trends was 24 μm, the standard deviation was 29 μm and the maximum unsigned difference was 88 μm.

Another trend was observed in the DoDs, after alignment and differentiation of the measured DEMs with the ground-truth DEM (Fig. 4). The trend is comparable to the material thermal contraction which caused the curvature observed during the drying process for the 3D printed model. The deviation of the final 3D printed model from its initial

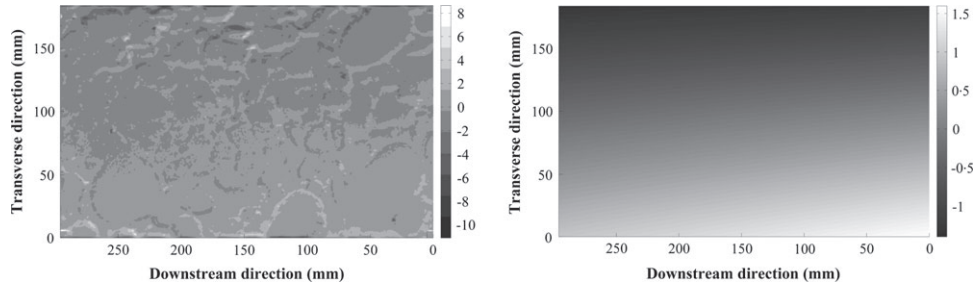

FIG. 3. (a) DEM of difference (DoD) before vertical alignment of the measured DEM collected with a 0·25 mm sampling distance with the ground-truth DEM. (b) Fitted bilinear trend representing the vertical misalignment of the stereo set-up. Elevations are displayed as gradient of greys; values are in millimetres.

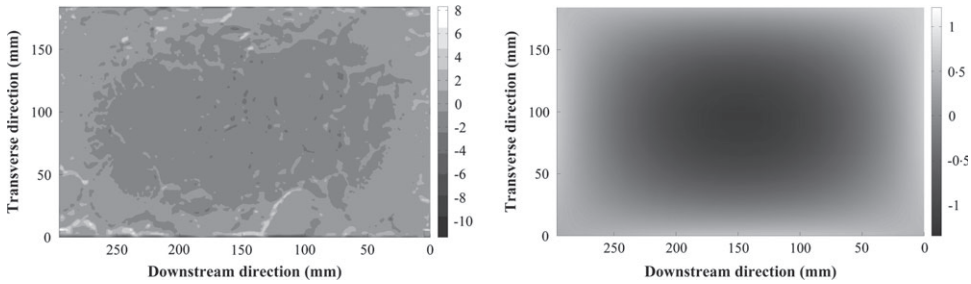

FIG. 4. (a) DEM of difference (DoD) before removal of the manufacturing-induced trend. (b) Fitted manufacturing-induced curvature that could not be eliminated by fixing the 3D printed model to a flat Perspex plate. Elevations are displayed as gradient of greys and values are in millimetres.

topography was measured with high precision by fitting a biquadratic surface to the DoDs using least squares. The magnitude of the deviation was found to be consistent throughout the various usages of the 3D printed model, exhibiting a mean absolute difference between two estimated trends (obtained using different set-up geometry) of 0·02 mm, a standard deviation of 0·03 mm and a maximum unsigned difference of 0·24 mm, suggesting that the curvature originated during manufacturing and remained constant afterwards. The shape (Fig. 4(a)), inherent to the 3D printed model, was obtained by averaging two estimated trends and was incorporated in the ground-truth elevation matrix. The ground-truth DEM now represented the actual 3D printed model.

To confirm that the curvature trend observed in the DoDs did not originate from the measurements, but was indeed inherent to the 3D printed model, a stereopair of the flat calibration chequerboard was matched with the SDPS. After alignment of the chequerboard's surface with the cameras' image plane using bilinear de-trending, a range of elevations of 0·4 mm (which is exactly the theoretical accuracy of the set-up and about 15% of the range of elevations found in Fig. 4) characterised the chequerboard surface and no clear trend was observed.

Assessment of Stereomatching Reliability

Quantitative evaluation and comparison of matching errors in DEMs of the 3D printed model and DEMs of the gravel bed was performed using the five DEMs that were collected for each case. It is important to note that the gravel-bed surface differs from the 3D printed model, although they share some common properties (the same sediment mixture and the same armouring process). The motivation of this test was to examine whether the 3D printed model is suitable as a real gravel bed substitute in terms of stereomatching.

The five DEMs were the result of matching stereopairs taken continuously (Fig. 5), and rectified with the same calibration results. Matching performance between stereopairs will thus only differ because of differences in the images themselves. Fig. 5(b) reveals that image data acquired with a 2 s interval timer differ, although variations are small (the standard deviation in overall pixel intensity (averaged over a given image) between the five images was of the order of 0·01). However, intensity variations between repeat photographs at some pixel locations are larger than one, and influenced the stereomatching. Pixel intensity is defined as the maximum tonal value between the red, green and blue channels,

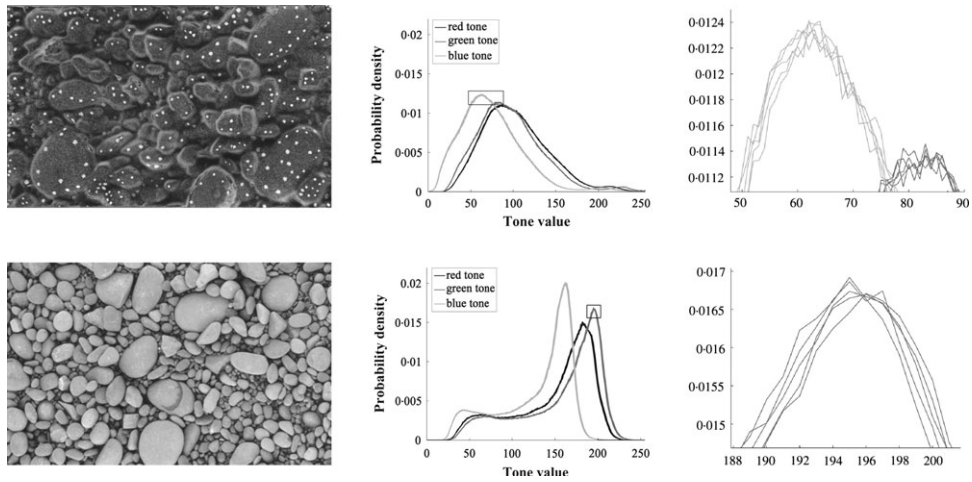

FIG. 5. Example of photographs (left), and image histograms (middle) in the red, green and blue channels, for the five left-hand images, reduced to the zones of interest shown in the photographs of (top) the 3D printed model and (bottom) the gravel bed. The enlargements on the right show the small differences between images.

expressed on an 8-bit (0 to 255) scale. The neon lights were identified as the cause of these differences, as they consist of periodic light stripes. Because the left-hand images are not consistent (idem with the right-hand images), the similarity in intensity (area-based) between the left and the right images may change between stereopairs (Table IV).

The five DEMs were differentiated one by one to provide a measure of the repeat stereomatching error value (RSEV) over the investigated surface. This procedure is similar to the use of the "repeat scan error value" by Hodge et al. (2009). Here, RSEV is a matrix, the same size as the measured data, containing the mean absolute height discrepancies at the grid nodes between all repeated measurements. In the case of five repeated measurements, this leads to 10 independent comparisons (Fig. 5). The RSEV was calculated as:

TABLE IV. Area-based differences in pixel intensity between the two images forming a stereopair, for the five stereopairs taken in a row, with evaluation limited to the zones of interest shown in Fig. 5.

Difference in the mean pixel intensity		*Difference in the median pixel intensity*	
3D printed model	*Gravel bed*	*3D printed model*	*Gravel bed*
0·45	0·80	0	0
0·44	0·79	1	0
0·45	0·77	0	0
0·44	0·79	1	0
0·45	0·80	1	0

$$\mathrm{RSEV}(x,y) = \frac{\sum_{i=1}^{5}\sum_{j=1}^{5}\left|z_i(x,y) - z_j(x,y)\right|}{10}, \quad \forall (i,j) \in [1,5] \text{ with } i \neq j$$

where $z_i(x, y)$ is the elevation at the grid node with coordinates (x, y) in scan or stereomatch i. Both the mean RSEV (after averaging the height differences over the grid) and the maximum RSEV were calculated over the 3D printed model and the gravel bed for various DEM sampling distances (from 0·25 to 3 mm), providing an estimate of stereomatching reliability over the two surfaces.

Results

Qualitative Evaluation of DEM Generation Using Default Sampling Distance

Fig. 6 presents DEMs obtained from recorded data of the 3D printed model and gravel bed, collected with a 0·25 mm sampling distance. The associated probability density functions (PDFs) of surface elevations are shown. Visually, both DEMs correctly represent the surface investigated. However, the enriched texture and greater colour range in images of the gravel bed are thought to contribute to a "sharper" graphical representation of the gravel-bed DEM.

Fig. 6 also shows that the recorded surface of the 3D printed model has a larger range of elevations with a narrower distribution around the zero-mean than the measured surface of the "real" gravel bed. This infers that the effect of water-working was stronger on the surface replicated by 3D printing, which agrees well with the visual observation of coarser exposed particles and thus deeper troughs between particles, compared to the "real" gravel bed.

Quantitative Assessment of DEM Quality

Fig. 7 shows the DoD (absolute differences are represented for clarity) obtained from the differentiation of the measured DEM (top left), after horizontal and vertical alignment, with the ground-truth DEM (top right), over the full dimensions of the 3D printed model. Visually, the two DEMs do not display obvious differences and analysis of the DoD is required. The DoD shows that surface errors are located at the grains' edges and gaps between grains. This observation relates well with findings obtained by Chandler et al. (2001), where stereomatching outliers were found near deep crevices between grains at the surface of a gravel bed. The reason is that occluded regions in the imagery, where pixels are replaced by values interpolated from neighbouring data, based on the assumption of a continuous surface, are smoothed in the DEMs and introduce surface errors.

Table V shows statistics on the surface error, obtained from the comparison of the elevations contained in the DEM collected with default parameters with the ground-truth elevations, over all check points (n = 873 345). There is little systematic error in the measured surface, witnessed by a ME which is close to zero. In this study, computations of the mean height discrepancies between the measurements and ground truth confirm that the vertical alignment was correctly performed. In the case of DEMs registered with an external coordinate system, such as by using total stations, evaluation of the ME can provide information on the presence of systematic shifts in the recorded elevations (Butler et al., 1998; 2002; Lane et al., 2000; Carbonneau et al., 2003).

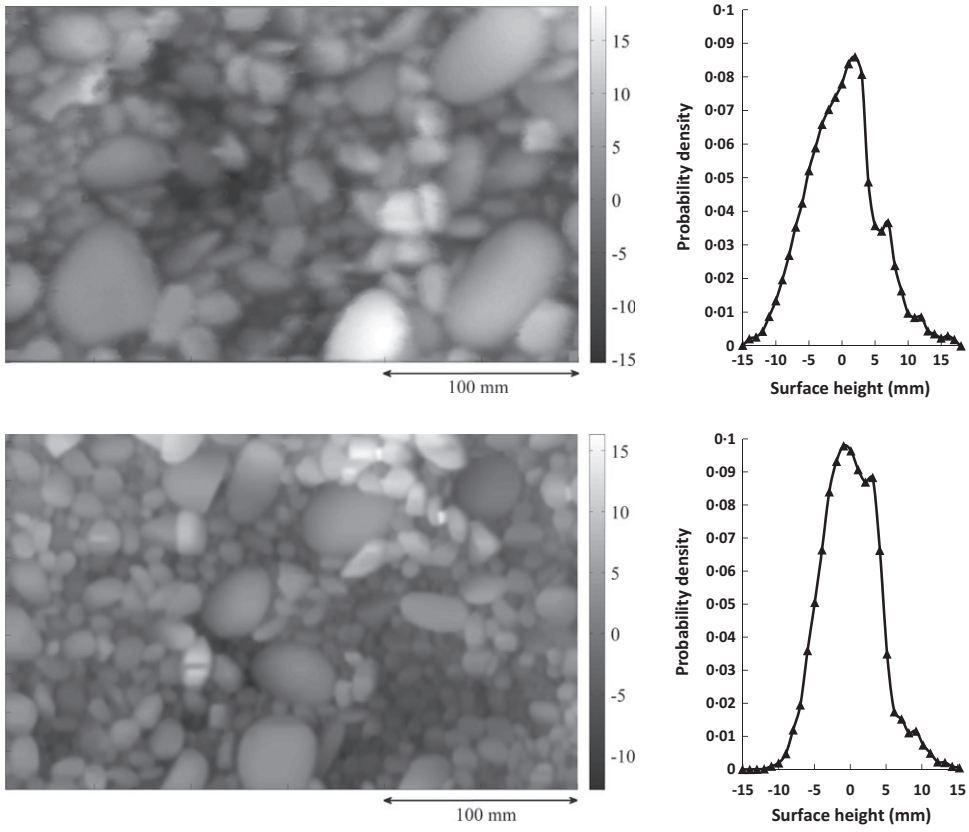

FIG. 6. 2·5D DEMs collected with 0·25 mm sampling distance of (top) the 3D printed model and (bottom) the gravel bed. Elevations are in millimetres and are represented with a gradient of greys. On the right are the associated PDFs of the DEM elevations.

The evaluation of the average surface error, represented by a mean unsigned, or absolute, error (MUE) of 0·43 mm, is needed to characterise the DEM accuracy. The global surface precision is characterised by a standard deviation of 0·62 mm (≃5% of surface D_{50}). Most DEM points (90%) are within ±1 mm of check points, and 0·5% of DEM points exhibit errors above 3 mm (Fig. 7, bottom).

The quality of the "default" DEM is encouraging, as the actual accuracy of the measurements, represented by a MUE of 0·43 mm, is not severely degraded compared with the theoretical vertical accuracy of 0·39 mm, and is constrained by the image resolution. Fig. 7 confirms again that the loss in accuracy is associated with occlusions in the imagery, suggesting that the process steps undertaken to reconstruct the DEM were correctly executed, with minimal error propagation.

The quality of the DEM obtained in this study improves on previous photogrammetric measurements of gravel beds. However, any comparison is rather ambiguous, since the success rate of a photogrammetric survey essentially depends on the photogrammetric design and on the surface investigated, which differ between studies. In Carbonneau et al. (2003), MEs from −1·5 to +3·6 mm, with surface precisions (SDE) ranging from 2·1 to

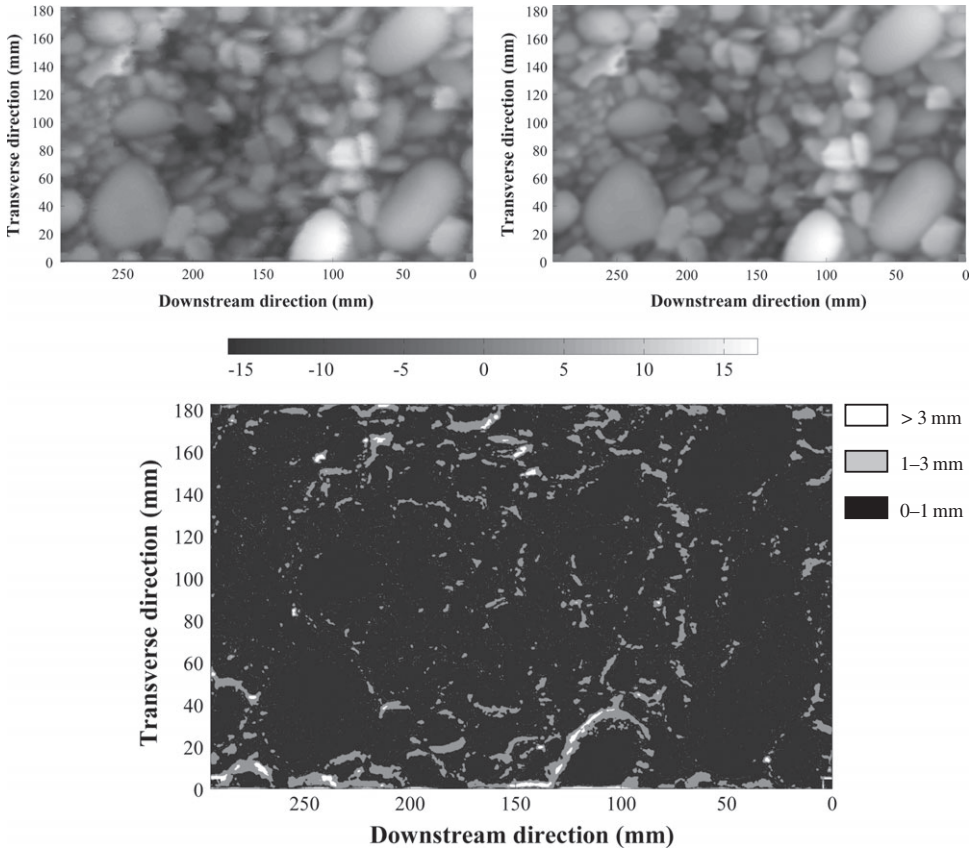

FIG. 7. Top left: measured DEM of the 3D printed model collected with a 0·25 mm sampling distance, horizontally and vertically aligned with the ground truth. Top right: ground-truth DEM. Bottom: DoD over the full dimensions of the 3D printed model. The same colour representation, with elevations in millimetres, is used to represent both the measured and the ground-truth DEMs.

8·5 mm, were associated with the measurement of a dry natural gravel bed in the field, with a camera-to-object distance of 1·1 m. The surveyed surfaces were made of larger grains, with a D_{50} ranging from 18 to 61 mm, compared with a D_{50} of 13 mm in the present study. In the laboratory, a RMSE of 1·7 mm was obtained with a camera "flying" height of 2 m by Chandler et al. (2001).

TABLE V. Quantitative assessment of the DEM collected with 0·25 mm sampling distance.

ME (mm)	0·04
MUE (mm)	0·43
SDE (mm)	0·62
Maximum absolute error (mm)	8·16
DEM points within ±0·5 mm of check points (%)	71·4
DEM points within ±1 mm of check points (%)	90·6
DEM points within ±3 mm of check points (%)	99·5

Effect of DEM Grid Size on DEM Quality

Fig. 8 presents the PDFs of surface error for various grid spacings. No difference is visible when the sampling distance is increased from 0·25 to 0·5 mm. Above 0·5 mm, there is a consistent increase in the vertical error with increasing sampling distance (Fig. 8). Thus, increasing DEM grid size significantly affects the DEM quality.

Fig. 9 shows the effect of DEM grid spacing on statistical quality measures of the DEMs obtained from a single stereopair and DEMs obtained from averaging five stereopairs. It can be seen that the surface errors do not vary with DEM averaging. Fig. 9 agrees well with Fig. 8 in that changing the sampling distance from 0·25 to 0·5 mm does not vary the DEM quality. When the sampling distance is increased beyond 0·5 mm, the DEM quality is reduced. In addition, the flattening of the graphs, with decreasing grid spacing, suggests that no improvement will result from reducing the sampling distance below 0·25 mm. This cannot be verified since check points for this study are sampled every 0·25 mm, and a denser grid of check points is needed to confirm this statement.

There is a direct correlation between the different statistical parameters and DEM grid size. A very small change is quantified when grid size is increased from 0·25 to 0·5 mm, with an improvement or deterioration of the parameters of less than 1%. An average deterioration of 9% is associated with an increase of the grid size from 0·25 to 0·75 mm (the deterioration is 10·6% in the MUE and 7·7% for the percentage of DEM points within ±0·5 mm of the reference ground-truth elevations). The deterioration is, on average, 34, 102 and 308% (with a standard deviation between parameters of 4·3, 13·4 and 33·8%), when the grid size is increased to 1, 1·5 and 3 mm, respectively.

Internal Reliability of Stereomatching

Fig. 10 presents the mean and maximum RSEVs for the DEMs of both the 3D printed model and the gravel bed, relating to different sampling distances. Overall, similar trends are observed, with reduced RSEVs for increased grid size. This is caused by smoothing

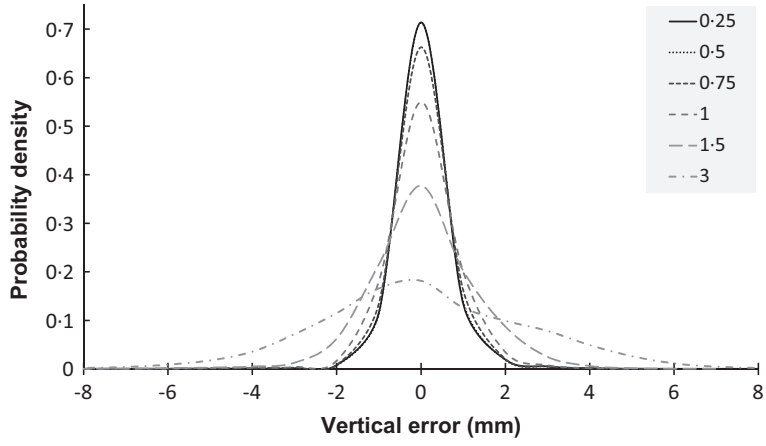

FIG. 8. Probability density functions (PDFs) of vertical error for different grid spacings from 0·25 to 3 mm. Surface error is normally distributed, resulting in a mean error close to zero. The PDFs for 0·25 and 0·5 mm grid spacings are virtually indistinguishable.

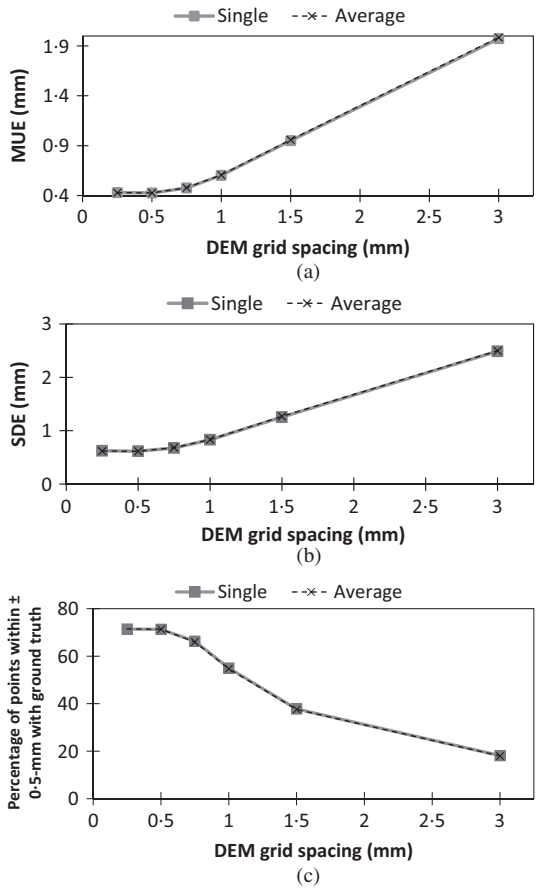

FIG. 9. Effects of DEM grid spacing and averaging DEMs collected from different imagery on statistical measures of DEM quality. *Single* refers to a single DEM whereas *average* corresponds to the gridded elevations of the five DEMs averaged to produce one DEM.

DEM matching errors, due to more point cloud data being used for interpolating elevations at grid nodes.

Figs. 10 and 11 and Table VI confirm that stereomatching is more consistent for data of the 3D printed model, compared to data of the gravel bed, with a mean RSEV reduced by 35%. Similarly, the maximum RSEV is larger for the gravel bed (4·59 mm) than for the 3D printed model (2·57 mm).

Finishing the surface of the 3D printed model maximised stereomatching performance, which is exemplified by a mean RSEV of 0·09 mm. However, the assessment of gravel-bed DEM quality using the 3D printed model results in accuracy statistics that may be understated (which means that DEM quality of a natural gravel bed is to be revised downwards), since errors due to stereomatching are globally lower in the DEMs of the 3D printed model.

The ratio of the mean RSEV (0·09 mm) to the MUE (0·43 mm) is approximately 1:5 for the DEMs of the 3D printed model. This confirms the observations made in previous

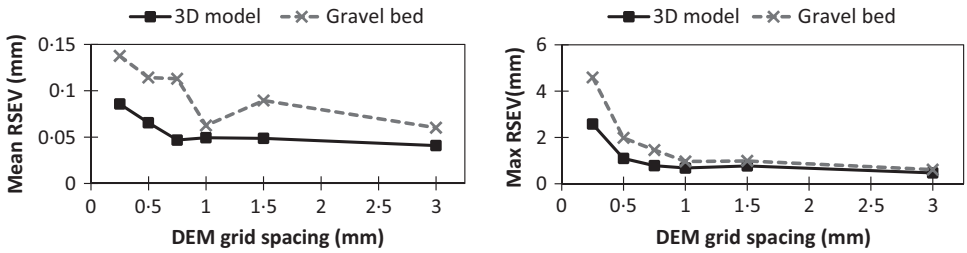

FIG. 10. Mean (left) and maximum (right) repeat stereomatching error value (RSEV) computed with 10 independent DEM comparisons for the 3D printed model and the gravel bed.

TABLE VI. Summary of RSEV for DEMs of 3D printed model and gravel bed collected with a 0·25 mm sampling distance.

	3D printed model	*Gravel bed*
Mean (mm)	0·09	0·14
Maximum (mm)	2·57	4·59
DEM points with RSEV ≤ 0·5 mm (%)	96·1	89·08
DEM points with RSEV ≤ 2 mm (%)	>99·99	99·93
DEM points with RSEV > 2 mm (%)	<0·01	0·07

studies (Butler et al., 1998), which suggested that image quality is an essential parameter in determining the success of photogrammetric surveys. However, image quality is often reduced to the texture contained in the imagery. Results of the present study, however, where DEMs are collected from different images of similar quality, suggest that intensity similarity between the two images forming a stereopair, on which stereo correspondence establishment relies, does affect DEM quality.

Whilst RSEVs cannot be ignored, especially at small sampling distances, averaging several DEMs collected from different imagery to mitigate stereomatching gross errors, proved to be of negligible interest in terms of measurement quality (Fig. 9). As an alternative, a filter, which removes and interpolates points in the average DEM, when RSEVs greater than 1 mm are detected, was tested on the DEM collected with default parameters. No significant change was observed. This is explained by the fact that stereomatching errors are essentially located in occluded regions of the DEM (Fig. 11), where elevations are already interpolated during stereomatching. Hence, a means to mitigate stereomatching errors in occluded regions of the DEMs has yet to be found, although the potential of multi-view stereo (MVS) methods might be investigated in this context.

DISCUSSION

Methods for assessing DEM quality, using independent check points, can easily result in misleading statistics, when the net of check points employed for the assessment is of low density and/or of poor repartition (Lane, 2000). Moreover, accuracy statistics might be insensitive to changes in DEM collection parameters. Another potential issue relates to the confidence with which check points are estimated and registered within the DEM. When measuring devices, such as total stations and laser scanners, are employed, errors can

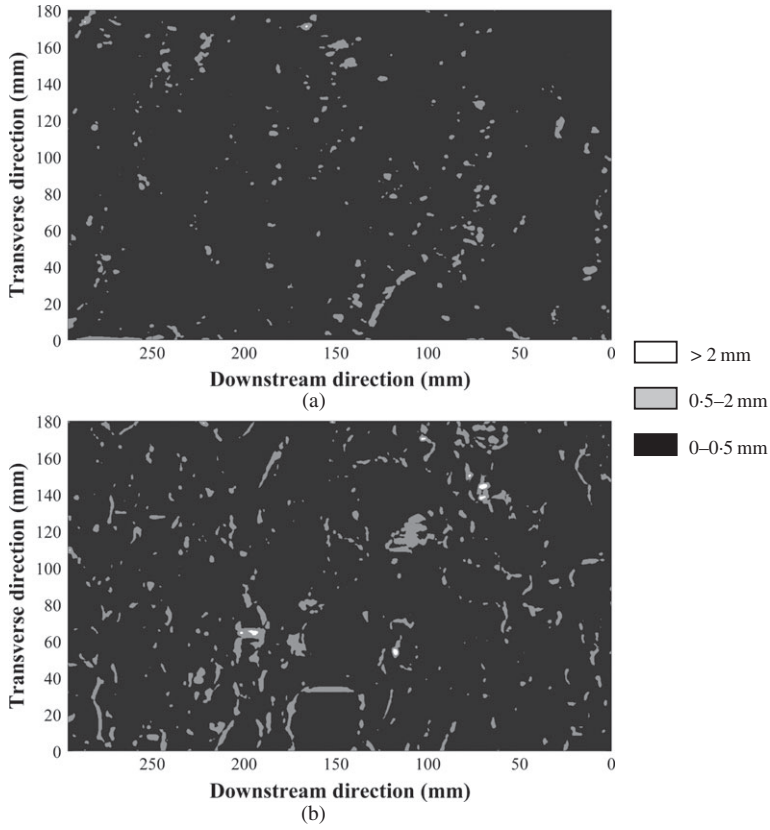

FIG. 11. Representation of the RSEV, which is the absolute difference between DEM points collected using different imagery, averaged over all 10 independent comparisons (five repeat DEMs), for (top) the 3D printed model and (bottom) the gravel bed. The sampling distance is 0·25 mm.

propagate so that the actual survey precision of check points is decreased and is generally not known.

The use of a 3D printed model to assess DEM quality improves greatly on previous approaches, which have been characterised by the need for an additional instrument to locate and register check points within the DEM. Furthermore, previously the preparation of ground-truth data has been repeated for each assessment and has required DEM reconstruction and error editing, which is time consuming. This has been replaced, in the current method, by the preparation of a reliable and practical 3D printed model. Thus, future studies are not restricted by the common characteristics of check point measuring devices, such as bulkiness and long recording times, which not only limits field applications, but also the ability to record underwater check points. In future, a 3D printed model provides a dense and accurate set of check data, where resolution is only limited by the 3D printer capabilities. In this study, the 3D printer would have allowed check points to be spaced with distances as small as 0·07 mm. This is beyond what is achievable with the measurement techniques currently used in hydraulic applications. Producing and handling such high-resolution data would still be difficult at present. In addition, the depth accuracy

with which the 3D model was printed, between 0·033 and 0·066 mm and with no error slip, ensured increased confidence in check point location. The size of the 3D printed model, 296 mm × 184 mm, which is the maximum size that the 3D printer available for the study allowed, might not be suitable for all applications. DEM quality assessment solutions over larger measurement windows are either: (a) to move the ground truth to determine the spatial distribution of DEM errors; or (b) to produce several ground-truth models that can be merged. However, the relatively small size of the model allows it to be used easily at various locations in the future, for both laboratory and field set-ups.

The main uncertainties in the assessment using a 3D printed model result from the alignment procedure necessary to superpose the measurements with the ground truth. These uncertainties were present when metrics obtained with stereo photogrammetry were compared with laser-scanned data (Lane, 2000; Chandler et al., 2001). In the present study, the alignment was performed using search and surface de-trending algorithms. The reliability of the procedure was assessed semi-independently by comparing the set-up vertical misalignment trends with different sampling distances. This demonstrated that the alignment procedure is able to align data with great precision, characterised in Table V by a ME of 0·04 mm.

The present work also highlights the challenges that larger rigid 3D printed models might face, due to the material's thermal contraction. There is limited information available on preparation that ensures minimal thermal contraction during the printing and drying phase. The observed deformation is largely dependent on the 3D printer and material used, and care needs to be taken to design a suitable model. In this study, the small warping effect the 3D print endured was corrected by mounting it on a flat and rigid Perspex sheet. The remaining trend of deformation was recorded by the set-up, and was confirmed by multiple recordings and corrected during post-processing.

The inherent difficulty related to the use of a 3D printed model to assess surface error is the need to produce a realistic model of the surface to survey, since a global measure of error can be unreliable if it is based upon test sites that have little resemblance with the site of interest (Lane et al., 2005; Wang et al., 2009). Topography has an essential impact on measurement quality, especially with photogrammetric surveys, with occluded regions accounting for most of the errors detected on the surface (Chandler et al., 2001). A realistic topography was acquired by measuring a patch of gravel bed, representative of simulated riverbeds in laboratory flumes. However, because the ground truth was acquired with imagery, the interstices between particles are not always represented accurately. A technique which allows vertical recording, such as laser scanning, if available, may theoretically improve the details at the interstices between particles of the ground truth. To obtain a natural look for the transparent 3D printer material, the gravel-bed model was painted and sand was spread on the wet paint to ensure reliable stereomatching on images of the 3D printed model (mean and maximum RSEV of 0·09 and 2·57 mm, respectively). The difference in stereomatching performance between images of the 3D printed model and those of a laboratory gravel bed was quantified in terms of the RSEV. This is proposed as an internal reliability test, addressing the stereomatching procedure. Larger RSEVs were obtained over the gravel bed (characterised by a 35% increase in mean RSEV), suggesting that stereomatching performs better, globally, over images of the 3D printed model. Hence, it is expected that DEM quality evaluated using the 3D printed gravel-bed model overestimates the DEM quality of natural gravel beds. For the 3D printed gravel-bed model, a ratio of 1:5 was obtained between the mean RSEV and the MUE. Assuming this ratio is valid for DEMs of natural gravel beds, this corresponds to an increase in the MUE from 0·43 mm for the 3D printed model to 0·7 mm for the natural gravel bed.

Conclusions

A 3D printed gravel-bed model was produced and subsequently used to evaluate the overall performance of a stereo-photogrammetric set-up developed for hydraulic experiments. The versatility and ease of use of the assessment method make it suitable to a large range of research areas, where small-scale and accurate topographic models are needed. The key advantages over traditional DEM evaluation methods can be summarised as follows:

(1) High density and uniform repartition of check points, which makes the DEM assessment more realistic and allows for a better quantification of errors due to changes in the DEM collection parameters, and as such allows optimisations to be performed on the photogrammetric workflow.
(2) Strong (and measurable) confidence in check point locations and registration with the measured DEM.
(3) Easier implementation of the assessment routine in a DEM acquisition campaign, with significant improvements in time and efficiency, and a larger range of situations where the assessment can be performed.

The results in this paper will be useful for setting up the optimum strategy for gravel-bed DEM collection, both in air and through water. Experiments have confirmed that the grid spacing should be chosen with care, in order to ensure correct surface representation. In particular, a sampling distance larger than 0·5 mm resulted in a significant loss of geometric information and degraded the DEM quality. Furthermore, it has been shown that the ground truth needs to be representative of the surface under consideration, in order to obtain the most realistic assessment. 3D printing is suitable, and at present the most advanced method, for obtaining realistic ground truth for known surfaces, although printed models can be affected by the material's thermal contraction. The acquisition of ground truth with imagery affects the surface details at interstices between particles.

The assessment of using off-the-shelf processing and consumer-grade digital cameras for a stereo-photogrammetric set-up showed that high accuracy and precision, in terms of sub-millimetre MUE and SDE, can be obtained with the presented default DEM collection parameters. Finally, this research confirmed the common expectation that most of the errors are caused by occluded regions in the imagery, a recurring stereo-photogrammetric measurement problem on rough surfaces. This suggests that new means for capturing occlusion, beyond traditional uniform surface smoothing, must be envisaged and the potential of employing MVS methods to assist in this regard may be worthy of investigation. The ultimate goal is to obtain measurements with local vertical accuracy as close as possible to the optimal accuracy allowable by the set-up.

Acknowledgement

The authors would like to thank the Editor, Stuart Granshaw, and two anonymous reviewers for their valuable comments, which helped to improve the paper.

References

Bertin, S., Friedrich, H., Chan, E. and Delmas, P., 2012. The development and internal assessment of a high-resolution, non-proprietary, stereo-photogrammetric setup for hydraulic experiments. *27th Conference on Image and Vision Computing New Zealand*, Dunedin, New Zealand. 515–520.

BERTIN, S. and FRIEDRICH, H., 2014. Measurement of gravel-bed topography: an evaluation study applying statistical roughness analysis. *Journal of Hydraulic Engineering*, 140(3): 269–279.

BOUGUET, J.-Y., 2010. http://www.vision.caltech.edu/bouguetj/calib_doc/ [Accessed: 1st July 2013].

BOURATSIS, P., DIPLAS, P., DANCEY, C. L. and APSILIDIS, N., 2013. High-resolution 3-D monitoring of evolving sediment beds. *Water Resources Research*, 49(2): 977–992.

BRASINGTON, J. and SMART, R. M. A., 2003. Close range digital photogrammetric analysis of experimental drainage basin evolution. *Earth Surface Processes and Landforms*, 28(3): 231–247.

BUTLER, J. B., LANE, S. N. and CHANDLER, J. H., 1998. Assessment of DEM quality for characterizing surface roughness using close range digital photogrammetry. *Photogrammetric Record*, 16(92): 271–291.

BUTLER, J. B., LANE, S. N. and CHANDLER, J. H., 2001. Characterization of the structure of river-bed gravels using two-dimensional fractal analysis. *Mathematical Geology*, 33(3): 301–330.

BUTLER, J. B., LANE, S. N., CHANDLER, J. H. and PORFIRI,, E., 2002. Through-water close range digital photogrammetry in flume and field environments. *Photogrammetric Record*, 17(99): 419–439.

CARBONNEAU, P. E., LANE, S. N. and BERGERON, N. E., 2003. Cost-effective non-metric close-range digital photogrammetry and its application to a study of coarse gravel river beds. *International Journal of Remote Sensing*, 24(14): 2837–2854.

CHANDLER, J. H., SHIONO, K., RAMESHWAREN, P. and LANE, S. N., 2001. Measuring flume surfaces for hydraulics research using a Kodak DCS460. *Photogrammetric Record*, 17(97): 39–61.

CHANDLER, J. H., BUFFIN-BÉLANGER, T., RICE, S., REID, I. and GRAHAM, D. J., 2003. The accuracy of a river bed moulding/casting system and the effectiveness of a low-cost digital camera for recording river bed fabric. *Photogrammetric Record*, 18(103): 209–223.

COOPER, M. A. R. and CROSS, P. A., 1988. Statistical concepts and their application in photogrammetry and surveying. *Photogrammetric Record*, 12(71): 637–663.

DETERT, M. and WEITBRECHT, V., 2012. Automatic object detection to analyze the geometry of gravel grains – a free stand-alone tool. *Proceedings of River Flow 2012*, San Jose, Costa Rica. 595–600.

FUSIELLO, A., TRUCCO, E. and VERRI, A., 2000. A compact algorithm for rectification of stereo pairs. *Machine Vision and Applications*, 12(1): 16–22.

GIMEL'FARB, G., 2002. Probabilistic regularisation and symmetry in binocular dynamic programming stereo. *Pattern Recognition Letters*, 23(4): 431–442.

GOOCH, M. J., CHANDLER, J. H. and STOJIC, M., 1999. Accuracy assessment of digital elevation models generated using the Erdas Imagine OrthoMAX digital photogrammetric system. *Photogrammetric Record*, 16(93): 519–531.

HODGE, R., BRASINGTON, J. and RICHARDS, K., 2009. In situ characterization of grain-scale fluvial morphology using terrestrial laser scanning. *Earth Surface Processes and Landforms*, 34(7): 954–968.

LANE, S. N., 2000. The measurement of river channel morphology using digital photogrammetry. *Photogrammetric Record*, 16(96): 937–961.

LANE, S. N., JAMES, T. D. and CROWELL, M. D., 2000. Application of digital photogrammetry to complex topography for geomorphological research. *Photogrammetric Record*, 16(95): 793–821.

LANE, S., CHANDLER, J. and PORFIRI, K., 2001. Monitoring river channel and flume surfaces with digital photogrammetry. *Journal of Hydraulic Engineering*, 127(10): 871–877.

LANE, S. N., WESTAWAY, R. M. and HICKS, D. M., 2003. Estimation of erosion and deposition volumes in a large, gravel-bed, braided river using synoptic remote sensing. *Earth Surface Processes and Landforms*, 28(3): 249–271.

LANE, S. N., REID, S. C., WESTAWAY, R. M. and HICKS, D. M., 2005. Remotely sensed topographic data for river channel research: the identification, explanation and management of error. *Chapter 6 in Spatial Modelling of the Terrestrial Environment* (Eds. R. E. J. Kelly, N. A. Drake & S. L. Barr). Wiley, Hoboken, New Jersey, USA. 290 pages: 113–136.

MARION, A., TAIT, S. J. and MCEWAN, I. K., 2003. Analysis of small-scale gravel bed topography during armoring. *Water Resources Research*, 39(12): 1334–1345.

MATTHEWS, N. A., 2008. Aerial and close-range photogrammetric technology: providing resource documentation, interpretation, and preservation. Technical Note 428, US Department of the Interior, Bureau of Land Management, National Operations Center, Denver, Colorado, USA. 42 pages.

OCKELFORD, A.-M. and HAYNES, H., 2013. The impact of stress history on bed structure. *Earth Surface Processes and Landforms*, 38(7): 717–727.

POLLYEA, R. M. and FAIRLEY, J. P., 2012. Experimental evaluation of terrestrial LiDAR-based surface roughness estimates. *Geosphere*, 8(1): 222–228.

QIN, J., ZHONG, D., WANG, G. and NG, S. L., 2012. On characterization of the imbrication of armored gravel surfaces. *Geomorphology*, 159–160: 116–124.

Rice, S. P., Buffin-Bélanger, T. and Reid, I., 2014. Sensitivity of interfacial hydraulics to the microtopographic roughness of water-lain gravels. *Earth Surface Processes and Landforms*, 39(2): 184–199.

Rieke-Zapp, D. H., Rosenbauer, R. and Schlunegger, F., 2009. A photogrammetric surveying method for field applications. *Photogrammetric Record*, 24(125): 5–22.

Smith, M., Vericat, D. and Gibbins, C., 2012. Through-water terrestrial laser scanning of gravel beds at the patch scale. *Earth Surface Processes and Landforms*, 37(4): 411–421.

Wang, C.-C., Hefner, B. T. and Tang, D., 2009. Evaluation of laser scanning and stereo photography roughness measurement systems using a realistic model seabed surface. *IEEE Journal of Oceanic Engineering*, 34(4): 466–475.

Zhang, Z., 1999. Flexible camera calibration by viewing a plane from unknown orientations. *Proceedings of 7th IEEE International Conference on Computer Vision*. 666–673.

Résumé

L'utilisation de la stéréophotogrammétrie pour obtenir des modèles numériques d'élévation (MNE) destinés à l'analyse de la topographie de surface est devenue courante dans la recherche en hydraulique, y compris pour l'étude des lits de graviers grossiers. Cet article évalue la qualité d'un MNE à partir d'un modèle réaliste de lit de graviers imprimé en 3D, dont les élévations sont connues avec un pas d'échantillonnage de 0,25 mm, comme réalité de terrain. Deux caméras Nikon D5100 et un logiciel libre de photogrammétrie pour l'étalonnage de la camera et la reconstruction du MNE sont utilisés pour cette étude. Un MNE mesuré est comparé point par point avec la réalité de terrain, et il présente une exactitude importante. Les réalités de terrain imprimées en 3D permettent une évaluation rapide et souple de la qualité d'un MNE ainsi que de la sensibilité de ses erreurs aux changements de la topographie de surface et des paramètres d'acquisition. Elles permettent d'optimiser l'évaluation de l'étalonnage et de la qualité des images, ainsi que les stratégies de filtrage des erreurs. A terme, les modèles imprimés en 3D permettront de réduire les erreurs d'appariement stéréoscopique dans les régions cachées et de définir les stratégies les plus adaptées pour l'acquisition de MNE sur des lits de graviers, aussi bien à l'air libre que sous l'eau.

Zusammenfassung

In der hydraulischen Forschung wird die Stereophotogrammetrie zur Analyse der topographischen Oberfläche mit Hilfe Digitaler Höhenmodelle (DHMs) zunehmend populär. Dies gilt insbesondere für Gebiete mit Flusssteinen und grobem Kies. Die Qualität eines durch Stereophotogrammetrie erzeugten Höhenmodells wird mit Hilfe eines realistischen Flussbettmodells, das mit einem 3D Drucker erzeugt wurde, und dessen Höhenpunkte im Abstand von 0·25 mm als Sollwerte dienen, abgeschätzt. Zwei Nikon D5100 Kameras und nicht-firmeneigene photogrammetrische Software für die Kamerakalibrierung und DHM Erzeugung werden für diese Studie verwendet. Das gemessene DHM wird Punkt für Punkt mit den Sollwerten verglichen und zeigt eine sehr hohe Genauigkeit. 3D Drucke von Sollwerten erlauben eine schnelle und vielseitige Evaluierung von DHM Qualität und der Zuverlässigkeit in Abhängigkeit von Änderungen der Oberflächentopographie und der Erfassungsparameter. Das Verfahren hat das Potential die Evaluierungen von Kalibrierung, von Bildqualität, sowie von robusten Filtertechniken zu rationalisieren. Letztendlich können die gedruckten 3D Modelle helfen die Probleme der Stereozuordnung bei Verdeckungen zu untersuchen und eine geeignete Strategie zur DHM Erfassung eines Kiesbetts auch mit Mehrmedienphotogrammetrie zu entwickeln.

Resumen

En la investigación hidráulica se esta popularizando el uso de la fotogrametría para obtener modelos digitales de elevaciones (MDEs) para el análisis topográfico de las superficies. En este trabajo se evalúa la calidad de MDE usando como referencia un modelo impreso realista de un lecho de grava gruesa, con elevaciones conocidas cada 0,25 mm. En el estudio se usan dos cámaras Nikon D5100 y software no propietario para la calibración de las cámaras y le reconstrucción del MDE. El MDE medido se compara punto a punto con la referencia mostrando una precisión en la medición muy alta. La impresión en 3D de la referencia proporciona una rápida y versátil evaluación de la calidad del MDE y de la sensibilidad de sus errores a cambios en la superficie y a los parámetros en la reconstrucción. Tiene el potencial para optimizar las evaluaciones de calibración y calidad de la imagen, así como estrategias de filtrado de errores. Finalmente los modelos 3D impresos permitirán explorar la reducción de errores de correspondencia de imágenes y definir la estrategia más apropiada para la captura de lechos de grava, tanto en el agua como fuera de ella.

摘要

在水环境研究领域尤其是针对砾石层研究中,利用立体摄影测量获取*DEM*进行地形分析,是该领域研究的热点。本文利用*3D*打印技术制作高程分层为*0·25 mm* 的砾石层模型作为参考数据来' 评价*DEM*质量,采用两台*Nikon D5100* 相机以及具有相机标定和*DEM*重建功能的摄影测量软件来制作*DEM*。*DEM*和*3D*打印模型逐点进行比较,结果展示了立体摄影测量手段制作*DEM*具有较高的测量精度,且*DEM*误差和地表地形的变化、采集参数的变化有一定的相关性。因此快捷的*3D*打印技术使全面评价引起 *DEM* 误差的因素成为可能。*3D*打印技术可以同样可以评价相机检校、影像质量以及误差滤波策略等。最重要的是, *3D*打印技术可能会在降低遮挡地区的立体匹配误差、通过水中和空中进行砾石层 *DEM*的采集策略发挥作用。